

# Static Polarizabilities of Copper Cluster Monocarbonyls $\text{Cu}_n\text{CO}$ ( $n = 2\text{--}13$ ) and Selectivity of CO Adsorption on Copper Clusters

Zexing Cao,\* Yanjin Wang, Jun Zhu, Wei Wu, and Qianer Zhang

Department of Chemistry, State Key Laboratory for Physical Chemistry of Solid Surfaces, Xiamen University, Xiamen 361005, China

Received: March 21, 2002; In Final Form: June 11, 2002

Density functional calculations for copper clusters  $\text{Cu}_n$  and their monocarbonyls  $\text{Cu}_n\text{CO}$  ( $n \leq 13$ ) have been performed using the relativistic ECP plus DZ basis set augmented by an  $f$  polarization function for copper atom. Equilibrium geometries, harmonic frequencies, and static mean polarizabilities of  $\text{Cu}_n$  and  $\text{Cu}_n\text{CO}$  are determined. The feature of CO adsorption on the copper cluster and the effect of CO adsorption on stability and polarizability of the cluster are investigated. Calculations show that CO adsorption on copper clusters is selective in terminal coordination, and the favored adsorption sites are dominated by the local orientation of relevant frontier orbitals and the distribution of overall electrostatic potential surfaces of copper clusters. The interaction of  $\text{Cu}_n$  with CO in the copper cluster carbonyls leads to significant odd–even variations of the static polarizability differences between  $\text{Cu}_n\text{CO}$  and the separated components  $\text{Cu}_n$  and CO. Size dependences of cohesive energies, CO binding energies, and static mean polarizabilities have been explored.

## I. Introduction

In the past few years, the metal clusters have attracted considerable attention, both experimental and theoretical, because of their significant importance in catalytic processes<sup>1</sup> and organometallic chemistry.<sup>2</sup> The characterization of the metal clusters allows a better understanding of the physics and chemistry of surfaces and gives insight into fundamental properties of their nanoscale and bulk counterparts.

A large number of new experimental techniques<sup>3–8</sup> and theoretical calculations<sup>9–15</sup> have recently been applied to copper clusters with different sizes and charges as well as the copper-adsorbate systems. Recent multiple-collision-induced dissociation (MCID) experiments by Kruckeberg et al.<sup>16</sup> show that singly charged odd-size copper clusters  $\text{Cu}_n^+$  have higher dissociation energies than the average value of their even-size neighbors in their favored dissociation processes by neutral dimer evaporation for small odd-size clusters  $\text{Cu}_n^+$  with  $n = 3, 5, 7, 11$  and by neutral monomer evaporation for other clusters. They also found that the single-charged clusters  $\text{Cu}_n^+$  for  $n = 3, 9, 15$ , and 21 show high stability for such fragmentations. Similarly, anionic species  $\text{Cu}_7^-$ ,<sup>8</sup>  $\text{Cu}_5\text{CO}^-$ ,<sup>8</sup> and the neutral  $\text{Cu}_{16}\text{CO}$ <sup>7</sup> were found to have elevated stability. Such relatively high stability agrees with the closed electronic shells of 2, 8, 10, 18, and 20 valence electrons in the jellium model. Electronic shell closures and odd–even effects were observed in abundance in spectra of different charged states and in photoelectron spectroscopy, as well as in the reactivity for  $\text{Cu}_n$  to form  $\text{Cu}_n\text{CO}$ .<sup>3,4,7,14</sup>

Though many properties of copper clusters have been investigated experimentally in detail, little is known about general features of their electronic interactions, dissociation, and absorption behavior. To understand their microscopic features and correlation with the bulk state, much theoretical effect at various levels has been directed to small copper clusters and their carbonyls. Calaminici et al.<sup>12</sup> performed density functional

calculations for small copper clusters  $\text{Cu}_n$  up to  $n = 5$ . The structures and spectroscopic properties of such clusters are predicted. Balbuena et al.<sup>14</sup> carried out a systematic density functional theory study of copper clusters in linear, planar, and 3-D structures. Their study supports the validity of the cluster approach to improve the understanding of fundamental properties at interfaces. At the INDO/CI level, Persson et al.<sup>15</sup> proposed new parametrization for copper and they calculated spectroscopic properties of copper clusters  $\text{Cu}_n$  ( $n \leq 10$ ). Their study has been extended to  $\text{Cu}_{10}\text{CO}$  as model of CO adsorption on the Cu(100) surface. Nygren and Siegbahn<sup>9</sup> used ab initio methodologies to calculate dissociation energies of copper cluster carbonyls  $\text{Cu}_n\text{CO}$  and  $\text{Cu}_n\text{CO}^+$  with relaxed geometries of the copper clusters. Their calculated results show an agreement with the adsorption energy from surface science.

The noble metal Cu has an electronic configuration of a closed d shell  $3d^{10}$  and a single valence electron  $4s^1$ , and it is thus closely related to that of the alkali metals. Presumably, the copper clusters have certain similarities to the alkali-metal clusters in the electronic and geometrical structures. Recent density functional calculations by Calaminici et al.<sup>13</sup> present the first study of static polarizabilities and polarizability anisotropies of copper clusters  $\text{Cu}_n$  ( $n \leq 9$ ). The calculated polarizability per atom for bare copper clusters displays a similar trend as for sodium clusters. These theoretical studies on well-characterized clusters have provided details on electronic interactions which complement experimental investigations, even different theoretical predictions exist for the ground-state properties of several copper clusters.

In the current work, we present an extensive theoretical study of copper clusters and their monocarbonyls of up to thirteen Cu atoms within the density functional formalism. All these clusters were fully optimized, and vibrational frequencies, static polarizabilities, cohesive energies, and CO adsorption on the copper clusters were investigated.

\* Corresponding author. E-mail: zxcao@xmu.edu.cn.

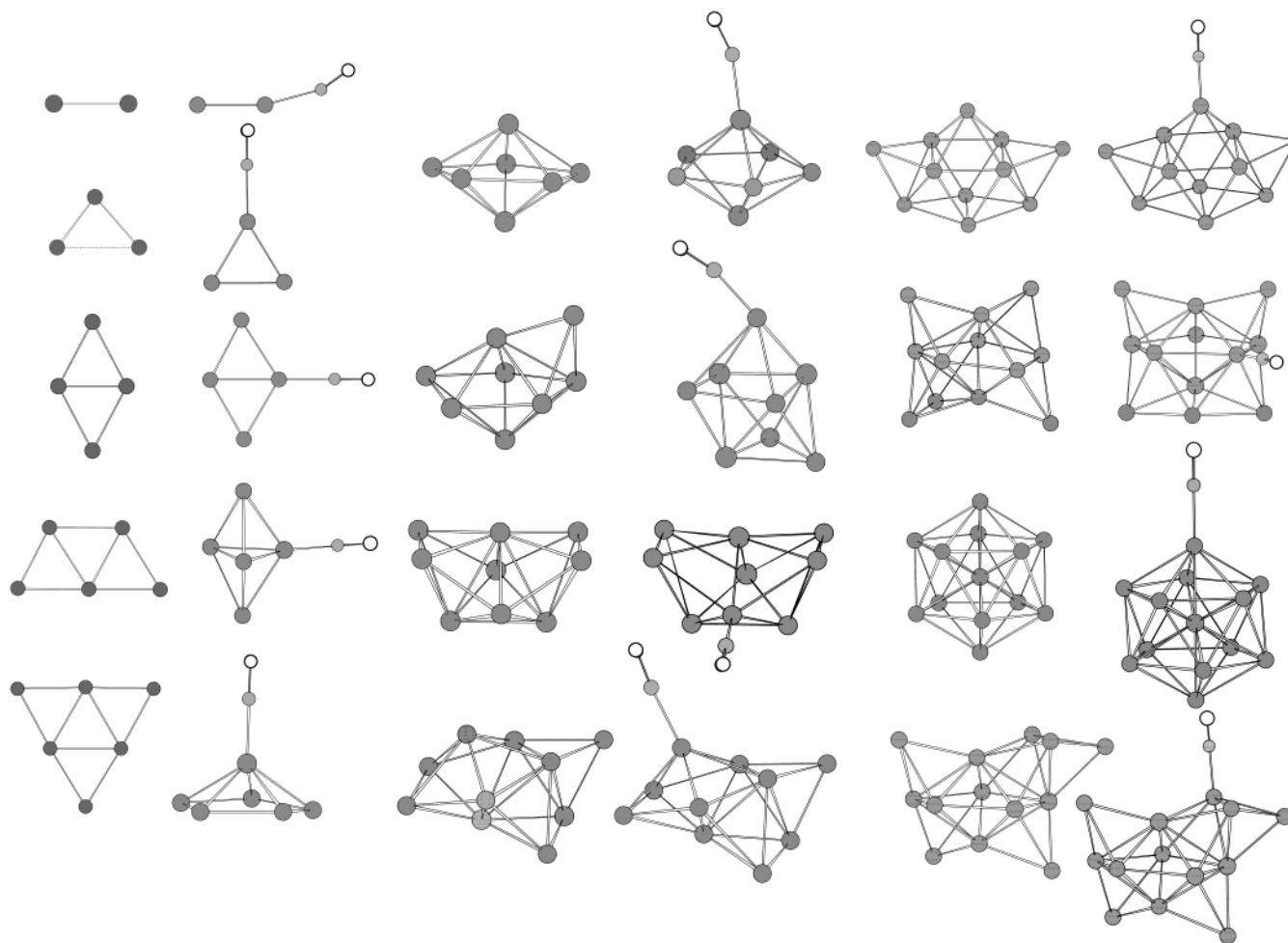


**Figure 1.** Structures of the ground states of  $\text{Cu}_n$  and  $\text{Cu}_n\text{CO}$  ( $n \leq 13$ ) clusters.

## II. Computational Details

The electronic structure of transition-metal clusters is very complicated, and reliable study from the first principle is rather demanding computationally. Presently, the density functional theory techniques, combined with relativistic effective core potentials, seem to be the most practicable tool to deal with these metal clusters. To calibrate the accuracy of this approach, we calculated spectroscopic parameters of  $\text{Cu}_2$  and its anion by the B3LYP functional<sup>17,18</sup> with Los Alamos ECP plus DZ basis set<sup>19</sup> augmented with an  $f$  polarization function<sup>20</sup> for copper. B3LYP calculated results in Table 1 show good agreement with experimental values. In the present study, the B3LYP functional with the relativistic ECP plus DZ basis set augmented with an  $f$  polarization function is used for all geometry optimization and frequency calculations. The 6-311G\* basis set is used for C and O atoms.

The mean polarizability was calculated from the polarizability components as

$$\bar{\alpha} = \frac{1}{3}(\alpha_{xx} + \alpha_{yy} + \alpha_{zz})$$

The basic quantity for discussing the stability of clusters is the cohesive energy  $\epsilon_{\text{coh}}$  defined as

$$\epsilon_{\text{coh}} = -[E(\text{Cu}_n) - nE(\text{Cu})]/n$$

Here, only electronic effects are considered and the zero point vibrational energy (ZPE) is not included. Actually, the ZPE

**TABLE 1: Comparison of the Calculated and Experimental Spectroscopic Parameters for the Ground State of  $\text{Cu}_2$  and  $\text{Cu}_2^-$**

species	bond lengths (Å)		frequencies (cm <sup>-1</sup> )		$D_e$ (eV)	
	B3LYP	exp	B3LYP	exp.	B3LYP	exp
$\text{Cu}_2$	2.26	2.22 <sup>a</sup>	256	265 <sup>a</sup>	2.02	2.08 <sup>c</sup>
$\text{Cu}_2^-$	2.39	2.35 <sup>b</sup>	191	210 ± 15 <sup>b</sup>	1.88	1.64 ± 0.15 <sup>d</sup>

<sup>a</sup> From ref 37. <sup>b</sup> From ref 38. <sup>c</sup> From ref 39. <sup>d</sup> From ref 8.

effects in such metal clusters are neglectable. All calculations were performed using the Gaussian-98 programs.<sup>21</sup>

## III. Results and Discussion

**A. Bare Copper Clusters. 1. Structures and Stabilities.** The most stable structures located by B3LYP calculations for copper clusters are displayed in Figure 1. The optimized Cu–Cu distances in these structures vary from 2.26 to 2.80 Å. Vibrational frequency analyses show that all structures are stable on the potential energy surfaces.  $\text{Cu}_2$  has a ground state of  $^1\Sigma_g^+$  with a closed-shell configuration  $(3d^{10})(3d^{10})(4s\sigma_g^2)$ , and the B3LYP Cu–Cu bond length is 2.260 Å.  $\text{Cu}_3$  was characterized by extensive experiments<sup>22,23</sup> and theoretical calculations.<sup>12,24</sup> The ground state of  $\text{Cu}_3$  has a triangle structure in  $C_{2v}$  symmetry. Two short bond lengths and the long one, respectively, are 2.326 and 2.803 Å by the B3LYP calculation. This triangle structure in the  $^2B_2$  ground state is corresponding to a Jahn–Teller distortion of an equilateral triangle in the  $^2E'$  state. For  $\text{Cu}_4$ , a rhombus arrangement in the  $^1A_g$  state is the most stable structure

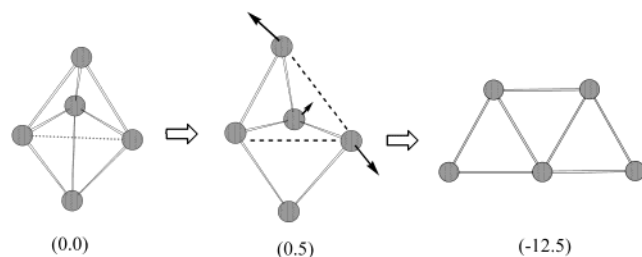


**Figure 2.** Conversion of the distorted trigonal bipyramid to the trapezoidal structure of  $\text{Cu}_5$ .

**TABLE 2: Calculated Cohesive Energies  $\epsilon_{\text{coh}}$  (in kcal/mol) and Static Mean Polarizabilities  $\bar{\alpha}$  (in au) of  $\text{Cu}_n$  ( $n = 2-13$ ) by the B3LYP Functional**

cluster	spin	$\epsilon_{\text{coh}}$	$\bar{\alpha}$
$\text{Cu}_2$	0	23.3	76.58 (78.50) <sup>a</sup>
$\text{Cu}_3$	1/2	23.2	131.57 (130.06)
$\text{Cu}_4$	0	30.1	153.82 (151.49)
$\text{Cu}_5$	1/2	32.6	195.60 (192.07)
$\text{Cu}_6$	0	36.7	221.37 (217.64)
$\text{Cu}_7$	1/2	37.4	241.70 (233.11)
$\text{Cu}_8$	0	39.3	272.94 (256.83)
$\text{Cu}_9$	1/2	39.0	309.93 (295.17)
$\text{Cu}_{10}$	0	40.2	346.31
$\text{Cu}_{11}$	1/2	40.6	373.10
$\text{Cu}_{12}$	0	40.7	424.70
$\text{Cu}_{13}$ (in $I_h$ symmetry)	5/2	40.0	410.90
$\text{Cu}_{13}$ (in $C_1$ symmetry)	1/2	41.1	465.30

<sup>a</sup> The values in parentheses are from ref 13.

by the B3LYP calculation, in agreement with previous theoretical studies.<sup>12,25</sup>

Current B3LYP calculations for  $\text{Cu}_5$  clusters found a trapezoidal  $C_{2v}$  structure in the  $^2A_1$  state as the most stable neutral pentamer, in agreement with previous LSD and GGA calculations.<sup>12</sup> However, a trigonal bipyramid structure was the most stable isomer for  $\text{Cu}_5$  in early theoretical calculations at various levels from semiempirical CNDO<sup>26</sup> to ab initio SCF method.<sup>27</sup> Present B3LYP calculations located a stable distorted trigonal bipyramid structure in the  $^2B_2$  state, lying about 12 kcal/mol above the most stable trapezoidal structure. The distorted trigonal bipyramid structure arises from a Jahn–Teller distortion of a  $D_{3h}$  trigonal bipyramid in the  $^2E'$  state, which is converted to the trapezoidal  $C_{2v}$  structure ( $^2A_1$ ) with a neglectable barrier of 0.5 kcal/mol at the B3LYP level. Figure 2 presents relative energies along the conversion process.

For  $\text{Cu}_6$  clusters, we found the  $^1A_1'$  state in  $D_{3h}$  symmetry as the ground state using the B3LYP functional, in agreement with previous calculations.<sup>13</sup> A pentagonal pyramid structure in  $C_{5v}$  symmetry is slightly higher in energy than the  $^1A_1'$  ground state by 5 kcal/mol. For  $\text{Cu}_7$ – $\text{Cu}_{13}$  clusters, a pentagonal bipyramid subunit can be found in their stable structures. Many experimental<sup>28,29</sup> and theoretical investigations<sup>30,31</sup> show that 5-fold symmetry is the natural choice of small microclusters of materials that crystallize in *fcc* lattices. Such structures are based on a centered 13-atom icosahedron, representing energy-preferred packing configuration in the metal cluster.

It is well known that transition-metal 13-atom clusters favor the  $I_h$  symmetry. For example, within the density functional formalism Reddy, Khanna, and Dunlap<sup>32</sup> find the  $I_h$  structure more stable than  $O_h$  for  $\text{Pd}_{13}$ ,  $\text{Rh}_{13}$ , and  $\text{Ru}_{13}$ , and giant magnetic moments are predicted for these metal clusters. We found a stable  $I_h$  structure for  $\text{Cu}_{13}$  in the  $^6A_g$  state with an electronic configuration  $\cdots(h_g)^5$  and the  $I_h$  structure is more stable than  $O_h$ . The higher stability of the  $I_h$  structure than  $O_h$  is also found for  $\text{Pd}_{13}$  at the SCF/CI level within the INDO model.<sup>33</sup> Notably,

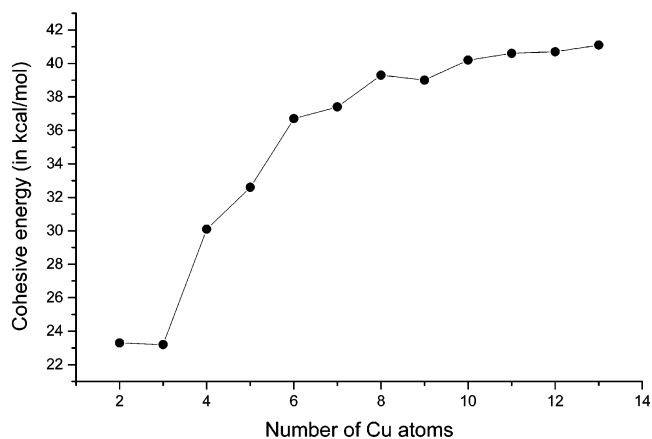


**Figure 3.** Calculated cohesive energies for  $\text{Cu}_n$  ( $n = 2-13$ ).

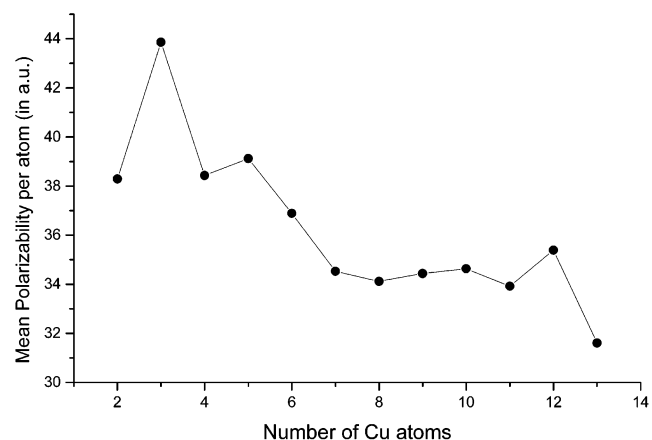


**Figure 4.** Calculated mean polarizability per atom of  $\text{Cu}_n$  ( $n = 2-13$ ).

our B3LYP calculations found a doublet state of  $\text{Cu}_{13}$  in  $C_1$  symmetry more stable than the  $I_h$  structure ( $^6A_g$ ) by about 14 kcal/mol. This  $C_1$  isomer of  $\text{Cu}_{13}$  consists of one pentagonal bipyramid, one trigonal bipyramid, and several trigonal pyramid arrangements.

**2. Size Dependence of Cohesive Energies and Mean Polarizabilities.** In Table 2 and Figure 3, we present the cohesive energies  $\epsilon_{\text{coh}}$  and the static mean polarizations. The cohesive energy increases significantly first, and then this trend becomes slow as the cluster increases. As Table 2 shows, going from  $\text{Cu}_2$  to  $\text{Cu}_{13}$  (in  $C_1$  symmetry), the static mean polarizability of copper clusters increases monotonically, in agreement with previous calculations for  $\text{Cu}_n$  ( $n \leq 9$ ).<sup>13</sup> A similar behavior was observed for the static polarizability of sodium clusters.<sup>13</sup> Compared with the sodium clusters, the calculated polarizability values of copper clusters are much smaller, showing that the electronic structures of the copper clusters are much more compact than those of the sodium clusters, that is, in copper clusters the electrons are more strongly attracted by the nuclei as in the sodium clusters. This difference in the electronic structure results in distinct properties in physics and chemistry between the bulk copper and sodium, even both have an  $ns^1$  configuration.

In Figure 4, the mean polarizability per atom of copper clusters is plotted, and an oscillation behavior is observed from  $\text{Cu}_2$  to  $\text{Cu}_{13}$ . For small clusters ( $n \leq 9$ ), the mean polarizability per atom of the odd-size cluster is relatively higher than that of the even-size cluster, which is consistent with an open-shell delocalization electronic structure for the odd-numbered cluster and a closed-shell configuration for the even-size cluster. With the increasing of the cluster size, the interactions of the electrons

**TABLE 3: Calculated CO Binding Energies  $E_b$  (in kcal/mol), Static Mean Polarizabilities  $\bar{\alpha}$  (in au) of  $\text{Cu}_n\text{CO}$  ( $n = 2-13$ ), and Static Mean Polarizability Differences  $\Delta\bar{\alpha}$  ( $\bar{\alpha}_{\text{Cu}_n\text{CO}} - \bar{\alpha}_{\text{Cu}_n} - \bar{\alpha}_{\text{CO}}$ ) by the B3LYP Functional<sup>a</sup>**

species	$E_b$	$\bar{\alpha}$	$\Delta\bar{\alpha}$
CO		10.18	
$\text{Cu}_2\text{CO}$	14.0	90.25	3.49
$\text{Cu}_3\text{CO}$	22.5	152.16	10.41
$\text{Cu}_4\text{CO}$	22.8	168.61	4.61
$\text{Cu}_5\text{CO}$	27.0	210.70	7.67 <sup>a</sup>
$\text{Cu}_6\text{CO}$	13.7	231.00	1.25 <sup>a</sup>
$\text{Cu}_7\text{CO}$	11.2	263.30	11.40
$\text{Cu}_8\text{CO}$	13.4	288.32	5.20
$\text{Cu}_9\text{CO}$	15.8	334.73	14.62
$\text{Cu}_{10}\text{CO}$	16.1	367.52	11.03
$\text{Cu}_{11}\text{CO}$	14.9	401.05	17.76
$\text{Cu}_{12}\text{CO}$	20.6	425.30	-9.58
$\text{Cu}_{13}\text{CO}$ (in $C_{5v}$ symmetry)	16.4	447.10	26.02
$\text{Cu}_{13}\text{CO}$ (in $C_1$ symmetry)	17.6	488.75	13.27

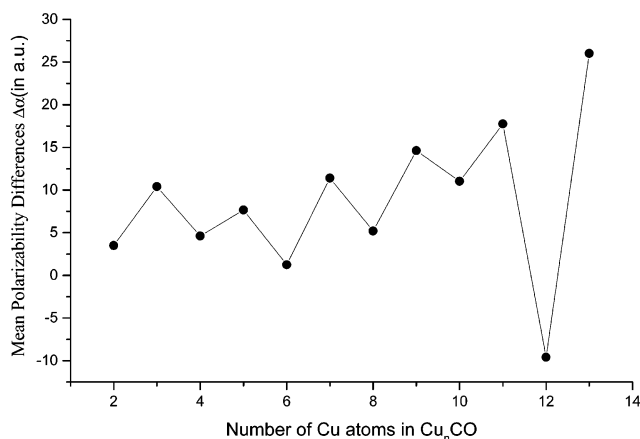
<sup>a</sup> An approximate trigonal bipyramid for  $\text{Cu}_5$  and a pentagonal pyramid for  $\text{Cu}_6$ , corresponding to the subunits in  $\text{Cu}_5\text{CO}$  and  $\text{Cu}_6\text{CO}$ , respectively, are used in calculation of CO binding energies and the static mean polarizability differences  $\Delta\bar{\alpha}$ .

with the nuclei in the clusters generally become stronger as the calculated cohesive energies show, which result in more compact electronic structure and make the mean polarizability per atom decrease overall. For larger copper clusters,  $\text{Cu}_{11}$  in  $C_{2v}$  symmetry and  $\text{Cu}_{13}$  in  $I_h$  symmetry have smaller the mean polarizability per atom than their even-size neighbors without symmetry. The  $C_1$  structure of  $\text{Cu}_{13}$  without symmetry has larger polarizability than the  $I_h$  structure, even the  $I_h$  structure has more unpaired electrons. These results show significant effect of the geometrical configuration on the polarizability for copper clusters.

**B. Copper Cluster Carbonyls. 1. Structures and Stabilities.** Carbonyls may be adsorbed on copper surfaces in terminal and bridged coordination and both sites show similar adsorption energies.<sup>34,35</sup> In this work, we focus on the terminal coordination. The most stable structures obtained by the B3LYP approach are incorporated into Figure 1 for comparison. Significant effects of association of CO to copper clusters on stabilities of certain copper cluster carbonyls have been noted. For example, the most stable structures for  $\text{Cu}_5\text{CO}$  and  $\text{Cu}_6\text{CO}$  are of distorted trigonal bipyramid and pentagonal pyramid copper framework, respectively, while bare copper clusters  $\text{Cu}_5$  and  $\text{Cu}_6$  have the most stable planar structures. Notable changes in geometry also take place in  $\text{Cu}_8\text{CO}$  and  $\text{Cu}_{12}\text{CO}$  in comparison with the frameworks of  $\text{Cu}_8$  and  $\text{Cu}_{12}$ . In other copper cluster carbonyls, the copper frameworks are less changed with association of CO.

**2. Size Dependence of CO Binding Energies and Mean Polarizabilities.** Table 3 collects the CO binding energies and the static mean polarizabilities of  $\text{Cu}_n\text{CO}$  up to  $n = 13$ . As Table 3 shows, the binding energies for the even-numbered copper carbonyls are in general slightly larger than that of the odd-size neighbors except  $\text{Cu}_5\text{CO}$ . Dissociation of  $\text{Cu}_5\text{CO}$  to  $\text{Cu}_5$  (in a distorted trigonal bipyramid) and CO requires a large energy of 27 kcal/mol. In consideration of the facile conversion from the distorted trigonal bipyramid to the trapezoidal  $C_{2v}$  structure as mentioned before, the dissociation energy is reduced to 15 kcal/mol. To examine effects of BSSE on the binding energies, we computed the counterpoise correction for  $\text{Cu}_4\text{CO}$ , and the BSSE correction reduces the binding energy by about 3 kcal/mol. For the copper cluster carbonyls, frequency calculations show that ZPE corrections lower the calculated binding energies by about 1 kcal/mol.

The static mean polarizability of  $\text{Cu}_n\text{CO}$  in Table 3 presents the same trend as bare copper clusters  $\text{Cu}_n$ , which increases

**Figure 5.** Calculated mean polarizability difference between  $\text{Cu}_n\text{CO}$  ( $n \leq 13$ ) and separated  $\text{Cu}_n$  and CO.**TABLE 4: Net Charges of CO, Selected DFT Bond Lengths (in Å), and Corresponding Vibrational Frequencies (in  $\text{cm}^{-1}$ ) of Copper Cluster Monocarbonyls**

cluster	spin	$q_{\text{CO}}$	$R_{\text{M-CO}}$	$R_{\text{C-O}}$	$\nu_{\text{M-CO}}$	$\nu_{\text{C-O}}$
$\text{Cu}_2\text{-CO}$	0	0.070	1.9562	1.1304	333	2179
$\text{Cu}_3\text{-CO}$	1/2	0.020	1.9040	1.1358	369	2113
$\text{Cu}_4\text{-CO}$	0	0.043	1.9061	1.1333	365	2152
$\text{Cu}_5\text{-CO}$	1/2	0.022	1.8854	1.1342	385	2142
$\text{Cu}_6\text{-CO}$	0	0.023	1.9177	1.1332	342	2151
$\text{Cu}_7\text{-CO}$	1/2	0.034	1.9788	1.1337	283	2130
$\text{Cu}_8\text{-CO}$	0	0.045	1.9812	1.1308	298	2165
$\text{Cu}_9\text{-CO}$	1/2	0.024	1.9414	1.1352	320	2117
$\text{Cu}_{10}\text{-CO}$	0	0.027	1.9299	1.1333	331	2144
$\text{Cu}_{11}\text{-CO}$	1/2	0.049	1.9498	1.1314	309	2152
$\text{Cu}_{12}\text{-CO}$	0	0.031	1.9315	1.1364	327	2116
$\text{Cu}_{13}\text{-CO}$	5/2	0.006	1.9311	1.1334	336	2132

monotonically, going from  $\text{Cu}_2\text{CO}$  to  $\text{Cu}_{13}\text{CO}$ . To get insight into the electronic structure of copper cluster carbonyls, we compute the static mean polarizability difference between  $\text{Cu}_n\text{-CO}$  and  $\text{Cu}_n + \text{CO}$ . As Table 3 and Figure 5 show, an odd-even alternation change exists for the polarizability differences  $\Delta\bar{\alpha}$ . The polarizability increment for the odd-numbered copper cluster carbonyl is larger than that of the even-numbered species. This result indicates that association of CO to the even-size copper clusters results in the electronic structure more compact than the odd-size copper clusters, especially for  $\text{Cu}_{12}\text{CO}$ , the  $\Delta\bar{\alpha}$  is negative. Interestingly, the mean polarizability of  $\text{Cu}_{13}\text{-CO}$  with an approximate  $I_h$  copper framework increases by 26 au in comparison with the separated  $\text{Cu}_{13}$  ( $I_h$ ) and CO, showing a strong electron delocalization between the surface Cu atoms and CO. In comparison with the sextet  $\text{Cu}_{13}\text{CO}$  in  $C_{5v}$  symmetry, the doublet  $\text{Cu}_{13}\text{CO}$  in  $C_1$  symmetry is more stable by 16 kcal/mol and has a larger mean polarizability of 488.75 au.

**3. Vibrational Frequencies of Adsorbed CO and Selectivity of CO Adsorption.** The optimized Cu-CO and C-O bond lengths and corresponding vibrational frequencies are presented in Table 4. Inspection of data in Table 4 reveals a strong correlation between bond length and stretching frequency for C-O as well as Cu-CO bond. The relationship between CO bond length and its vibrational frequency has been investigated in different carbonyl complexes.<sup>36</sup> To examine such relationship in copper cluster carbonyls, we performed a regression analysis based on the calculated results shown in Table 4, and the relationship may be expressed as

$$\ln \nu_{\text{CO}} = 12.84415 - 4.56555r_{\text{CO}}$$

There is a good linear correlation between the calculated CO bond length and the natural logarithm of frequency. This linear



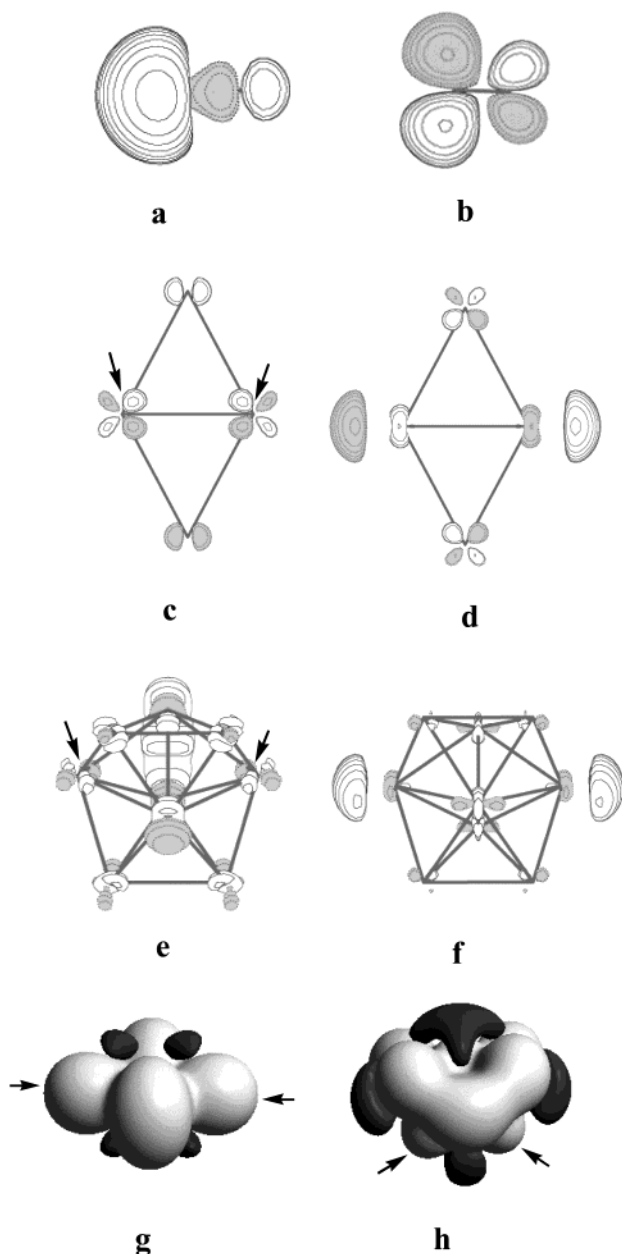


**Figure 6.** The frontier molecular orbitals and electrostatic potential surfaces (ESP): (a) HOMO of CO; (b) LUMO of CO; (c) HOMO of  $\text{Cu}_4$ ; (d) LUMO of  $\text{Cu}_4$ ; (e) the HOMO of  $\text{Cu}_9$ ; (f) LUMO of  $\text{Cu}_9$ ; (g) ESP of  $\text{Cu}_4$ ; (h) ESP of  $\text{Cu}_9$ . The blue and gray indicate negative and positive region, respectively, and favored site for CO adsorption is marked by arrow.

correlation in copper cluster carbonyls is similar to that in transition-metal carbonyl complexes,<sup>36</sup> suggesting that there is a similar bonding between the transition metal and CO in clusters and in compounds.

The net charges of CO presented in Table 4 show that partial electrons from CO are transferred to copper clusters in  $\text{Cu}_n\text{CO}$ , where CO behaves as a donor while  $\text{Cu}_n$  behaves as an acceptor in bonding between  $\text{Cu}_n$  and CO.

During the optimization of copper cluster carbonyls, we found that the stability of  $\text{Cu}_n\text{CO}$  strongly depends on the adsorption site on copper cluster carbonyls. For small copper clusters  $\text{Cu}_n$  up to  $n = 8$ , CO adsorption generally favors the electron-deficient site. However,  $\text{Cu}_9\text{CO}$  and  $\text{Cu}_{10}\text{CO}$ , formed by CO adsorbed on the most electron-deficient sites of  $\text{Cu}_9$  and  $\text{Cu}_{10}$ , have almost neglectable binding energies. To understand this

selectivity of CO adsorption on copper clusters, we analyze related frontier molecular orbitals and the overall electrostatic potential surfaces of  $\text{Cu}_n$ .

Figure 6 displays relevant frontier molecular orbitals and electrostatic potential surfaces (EPS) of  $\text{Cu}_4$  and  $\text{Cu}_9$ , where the favored adsorption sites are indicated with arrows. These HOMOs and LUMOs are located on active sites, respectively, and match the antibonding  $\pi^*$  (LUMO) and the HOMO  $\sigma$  molecular orbitals of CO very well, leading to strong donation-back-donation bonding attractions. On the basis of the features of related frontier molecular orbitals in other clusters, the stable copper cluster carbonyls are successfully located. The electrostatic potential in outer sphere of copper clusters in general is positive, and local negative parts are distributed in certain different regions. In the active site for CO adsorption, the positive and negative electrostatic potential distribution in space may match the  $\sigma$  donor and the  $\pi^*$  acceptor from CO, respectively. This local orientation of the overall electrostatic potential distribution of copper clusters, much like the spatial local distribution of relevant frontier molecular orbitals in the copper clusters, is relative to the selectivity of CO adsorption.

#### IV. Conclusions

In this work, we have performed extensive density functional calculations for the structures, static mean polarizabilities, vibrational properties, and CO adsorption on copper clusters  $\text{Cu}_n$  ( $n \leq 13$ ). DFT calculations show that all the ground-state geometries of the small clusters  $\text{Cu}_n$  ( $n \leq 6$ ) are planar. For the clusters  $\text{Cu}_n$  ( $n = 7-13$ ), a pentagonal bipyramid subunit exists in their stable structures. The association of CO to the copper clusters results in that frameworks of certain copper cluster carbonyls  $\text{Cu}_n\text{CO}$  ( $n = 5, 6, 8, 12$ ) in their ground states significantly differ from corresponding bare copper clusters.

The calculated static mean polarizability of  $\text{Cu}_n$  and  $\text{Cu}_n\text{CO}$  increases monotonically as the cluster increases, while the mean polarizability per atom has an oscillator behavior and the overall trend decreases with increasing of the cluster size. This is in agreement with the size dependence of the cohesive energy. This size dependence shows a compact electronic structure in the large copper cluster. In general, association of CO to copper clusters may enhance the static mean polarizability, especially, in the sextet  $\text{Cu}_{13}\text{CO}$  the  $\bar{\alpha}$  increases by about 26 au compared with separated components, showing that there is stronger electron delocalization between the surface Cu atoms with CO in the  $C_{5v}$  symmetry structure.

Present calculations show that CO adsorption on copper clusters in terminal coordination has selectivity, and the local symmetry of relevant frontier molecular orbitals and the orientation of the overall electrostatic potential surface are responsible for the selectivity. Calculated CO frequencies in the copper cluster monocarbonyls reveal a linear relationship between the natural logarithm of frequency and the CO bond length.

**Acknowledgment.** This work was financially supported from the National Science Foundation of China (Project Nos. 20173042 and 20021002) and the Ministry of Science and Technology of China (Project No. 001CB1089).

#### References and Notes

- (1) Somorjai, G. A.; Borodko, Y. G. *Catal. Lett.* **2001**, 76, 1.
- (2) Collman, J. P.; Hegedus, L. S.; Norton, J. R.; Finke, R. J. *Principles and Applications of Organotransition Metal Chemistry*; University Science Book: Mill Valley, CA, 1987.

- (3) Taylor, K. J.; Pettiette-Hall, C. L.; Cheshnovsky, O.; Smalley, R. E. *J. Chem. Phys.* **1992**, *96*, 3319.
- (4) Ho, J.; Ervin, K. M.; Lineberger, W. C. *J. Chem. Phys.* **1990**, *93*, 6987.
- (5) Jarrold, M. F.; Creegan, K. M. *Int. J. Mass Spectrom. Ion Processes* **1990**, *102*, 161.
- (6) Knickelbein, M. B. *Chem. Phys. Lett.* **1992**, *192*, 129.
- (7) Holmgren, L.; Grönbeck, H.; Aderson, M.; Rosen, A. *Phys. Rev. B* **1996**, *53*, 16644.
- (8) Spasov, V. A.; Lee, T.-H.; Ervin, K. M. *J. Chem. Phys.* **2000**, *112*, 1713.
- (9) (a) Nygren, M. A.; Siegbahn, P. E. M. *J. Phys. Chem.* **1992**, *96*, 7579. (b) Nygren, M. A.; Siegbahn, P. E. M.; Jin, C. M.; Guo, T.; Smally, R. E. *J. Chem. Phys.* **1991**, *95*, 6181.
- (10) Barnes, L. A.; Rosi, M.; Bauschlicher, C. W. *J. Chem. Phys.* **1990**, *93*, 609.
- (11) Jackson, K. A. *Phys. Rev. B* **1993**, *47*, 9715.
- (12) Calaminici, P.; Köster, A. M.; Russo, N.; Salahub, D. R. *J. Chem. Phys.* **1996**, *105*, 9546.
- (13) Calaminici, P.; Köster, A. M.; Vela, A. *J. Chem. Phys.* **2000**, *113*, 2199.
- (14) Balbuena, P. B.; Derosa, P. A.; Seminario, J. M. *J. Phys. Chem. B* **1999**, *103*, 2830.
- (15) Person, P.; Bustad, J.; Zerner, M. C. *Int. J. Quantum Chem.* **2000**, *21*, 1221.
- (16) Krückeberg, S.; Schweikhard, L.; Ziegler, J.; Dietrick, G.; Lützenkirchen, K.; Walther, C. *J. Chem. Phys.* **2001**, *114*, 2955.
- (17) Becke, A. D. *J. Chem. Phys.* **1993**, *98*, 5648.
- (18) Lee, C.; Yang, W.; Parr, R. G. *Phys. Rev. B* **1988**, *37*, 785.
- (19) Hay, J. P.; Wadt, W. R. *J. Chem. Phys.* **1985**, *82*, 299.
- (20) Höllwarth, A.; Böhme, M.; Dapprich, S.; Ehlers, A. W.; Gobbi, A.; Jonas, V.; Köhler, K. F.; Veldkamp, R.; Frenking, G. *Chem. Phys. Lett.* **1993**, *208*, 111.
- (21) Frisch, M. J. et al. *Gaussian 98*, revision A.7; Gaussian Inc.: Pittsburgh, PA, 1998.
- (22) Howard, J. A.; Preston, K. F.; Sutcliffe, R.; Mile, B. *J. Phys. Chem.* **1983**, *87*, 536.
- (23) Crumley, W. H.; Hayden, J. S.; Gole, J. L. *J. Chem. Phys.* **1986**, *84*, 5250.
- (24) (a) Walch, S. P.; Bauschlicher, C. W., Jr.; Langhoff, S. R. *J. Chem. Phys.* **1986**, *85*, 5900. (b) Bauschlicher, C. W., Jr.; Langhoff, S. R.; Partridge, H. *J. Chem. Phys.* **1990**, *93*, 8133.
- (25) Balasubramanian, K.; Feng, P. Y. *J. Phys. Chem.* **1990**, *94*, 1536.
- (26) Anderson, A. B. *J. Chem. Phys.* **1978**, *68*, 1744.
- (27) Bachmann, C.; Demuynek, J.; Veillard, A. *Faraday Symp. Chem. Soc.* **1980**, *14*, 170.
- (28) Rieck, D. F.; Gavney, J. A.; Norman, R. L.; Hayashi, R. K.; Dahl, L. F. *J. Am. Chem. Soc.* **1992**, *114*, 10369.
- (29) Zebrowsky, J. P.; Hayashi, R. K.; Dahl, L. F. *J. Am. Chem. Soc.* **1993**, *115*, 1142.
- (30) Cheng, H. P.; Berry, R. S.; Whetten, R. L. *Phys. Rev. B* **1991**, *43*, 10647.
- (31) Valkealahti, S.; Manninen, M. *Phys. Rev. B* **1992**, *45*, 9459.
- (32) Reddy, B. V.; Khanna, S. N.; Dunlap, B. I. *Phys. Rev. Lett.* **1993**, *70*, 3323.
- (33) Estiú, G. L.; Zerner, M. C. *J. Phys. Chem.* **1994**, *98*, 4793.
- (34) Ishi, S.; Ohno, Y.; Viswanathan, B. *Surf. Sci.* **1985**, *161*, 349.
- (35) Tracy, J. C. *J. Chem. Phys.* **1972**, *56*, 2748.
- (36) Niu, S. Q.; Thomson, L. M.; Hall, M. B. *J. Am. Chem. Soc.* **1999**, *121*, 4000.
- (37) Huber, K. P.; Herzberg, G. *Molecular Spectra and Molecular Structure-IV*; Van Nostrand-Reinhold: New York, 1989.
- (38) Leopold, D. G.; Ho, J.; Lineberger, W. C. *J. Chem. Phys.* **1987**, *86*, 1715.
- (39) Rohlfing, E. A.; Valentini, J. J. *J. Chem. Phys.* **1986**, *84*, 6560.